AGU PUBLICATIONS

Geophysical Research Letters

RESEARCH LETTER
10.1002/2017GL074725

Key Points:
- Our simulations produce pulse-like partial ruptures, confined to the higher stress zone at the edge of velocity-weakening areas
- The amplitude of high-frequency sources is enhanced in the zone of higher, heterogeneous stress at the edge of the velocity-weakening area
- Partial and full ruptures are possible if the nucleation size is small enough compared to the width of the velocity-weakening areas

Supporting Information:
- Supporting Information S1
- Movie S1
- Data Set S1
- Data Set S2
- Data Set S3

Correspondence to:
S. Michel,
sylvain_michel@live.fr

Citation:
Michel, S., J.-P. Avouac, N. Lapusta, and J. Jiang (2017), Pulse-like partial ruptures and high-frequency radiation at creeping-locked transition during megathrust earthquakes, *Geophys. Res. Lett.*, *44*, 8345–8351, doi:10.1002/2017GL074725.

Received 26 JUN 2017
Accepted 10 AUG 2017
Accepted article online 16 AUG 2017
Published online 31 AUG 2017

Pulse-like partial ruptures and high-frequency radiation at creeping-locked transition during megathrust earthquakes

Sylvain Michel[1,2], Jean-Philippe Avouac[2], Nadia Lapusta[2,3], and Junle Jiang[4]

[1]Bullard Laboratories, Department of Earth Sciences, University of Cambridge, Cambridge, UK, [2]Division of Geological and Planetary Sciences, California Institute of Technology, Pasadena, California, USA, [3]Division of Engineering and Applied Science, California Institute of Technology, Pasadena, California, USA, [4]Institute of Geophysics and Planetary Physics, Scripps Institution of Oceanography, University of California, San Diego, La Jolla, California, USA

Abstract Megathrust earthquakes tend to be confined to fault areas locked in the interseismic period and often rupture them only partially. For example, during the 2015 *M*7.8 Gorkha earthquake, Nepal, a slip pulse propagating along strike unzipped the bottom edge of the locked portion of the Main Himalayan Thrust (MHT). The lower edge of the rupture produced dominant high-frequency (>1 Hz) radiation of seismic waves. We show that similar partial ruptures occur spontaneously in a simple dynamic model of earthquake sequences. The fault is governed by standard laboratory-based rate-and-state friction with the aging law and contains one homogenous velocity-weakening (VW) region embedded in a velocity-strengthening (VS) area. Our simulations incorporate inertial wave-mediated effects during seismic ruptures (they are thus fully dynamic) and account for all phases of the seismic cycle in a self-consistent way. Earthquakes nucleate at the edge of the VW area and partial ruptures tend to stay confined within this zone of higher prestress, producing pulse-like ruptures that propagate along strike. The amplitude of the high-frequency sources is enhanced in the zone of higher, heterogeneous stress at the edge of the VW area.

1. Introduction

Megathrust earthquake ruptures are generally confined to areas of the plate interface that were previously locked [*Konca et al*., 2008; *Moreno et al*., 2010; *Loveless and Meade*, 2011; *Protti et al*., 2013], and they often rupture them only partially. The factors controlling the extent of such partial ruptures are unclear. The *M*7.8 Gorkha earthquake in Nepal of 25 April 2015 is a well-documented example of such a rupture (Figure 1) [*Avouac et al*., 2015; *Galetzka et al*., 2015; *Meng et al*., 2016]. It ruptured the Main Himalayan Thrust (MHT), the megathrust along which India is thrust under the Himalaya. The seismological and near-field high-rate geodetic records clearly show that it unzipped the lower edge of the locked portion of the fault, nucleating at 15 km depth and propagating eastward at ~2.8 km/s, in a pulse-like manner. High-frequency (HF) waves radiated from the lower edge of the rupture, tracking the pulse propagation (Figure 1a). Similar ruptures have been observed on subduction megathrusts, e.g., the M_w 7.7 Tocopilla earthquake offshore northern Chile in 2007 [*Béjar-Pizarro et al*., 2010] and M_w 7.7 Nazca earthquake offshore southern Peru in 1996 [*Pritchard et al*., 2007].

The factors that determine the extent of seismic ruptures remain poorly understood. They could reflect the geometry or heterogeneous frictional properties of the plate interface. For example, it has been proposed that the updip edge of the Gorkha rupture was arrested by a ramp along the MHT [*Hubbard et al*., 2016]. This scenario was demonstrated to be a reasonable possibility based on quasi-dynamic simulations [*Qiu et al*., 2016]. It is unlikely, however, that such a structural control would explain similar partial ruptures in the context of subduction megathrusts as ramp-and-flat systems are less likely to develop along the plate interface.

In this study, we investigate whether such partial ruptures and some of the specific characteristics of the Gorkha earthquake can be qualitatively reproduced without the need for any structural control. We resort to numerical simulations of earthquake sequences using the method of *Lapusta and Liu* [2009].

2. Model Setup

We assume that slip along the megathrust is governed by a rate-and-state friction law, as this framework has been shown to produce realistic models of earthquake sequences, aseismic slip, and individual ruptures

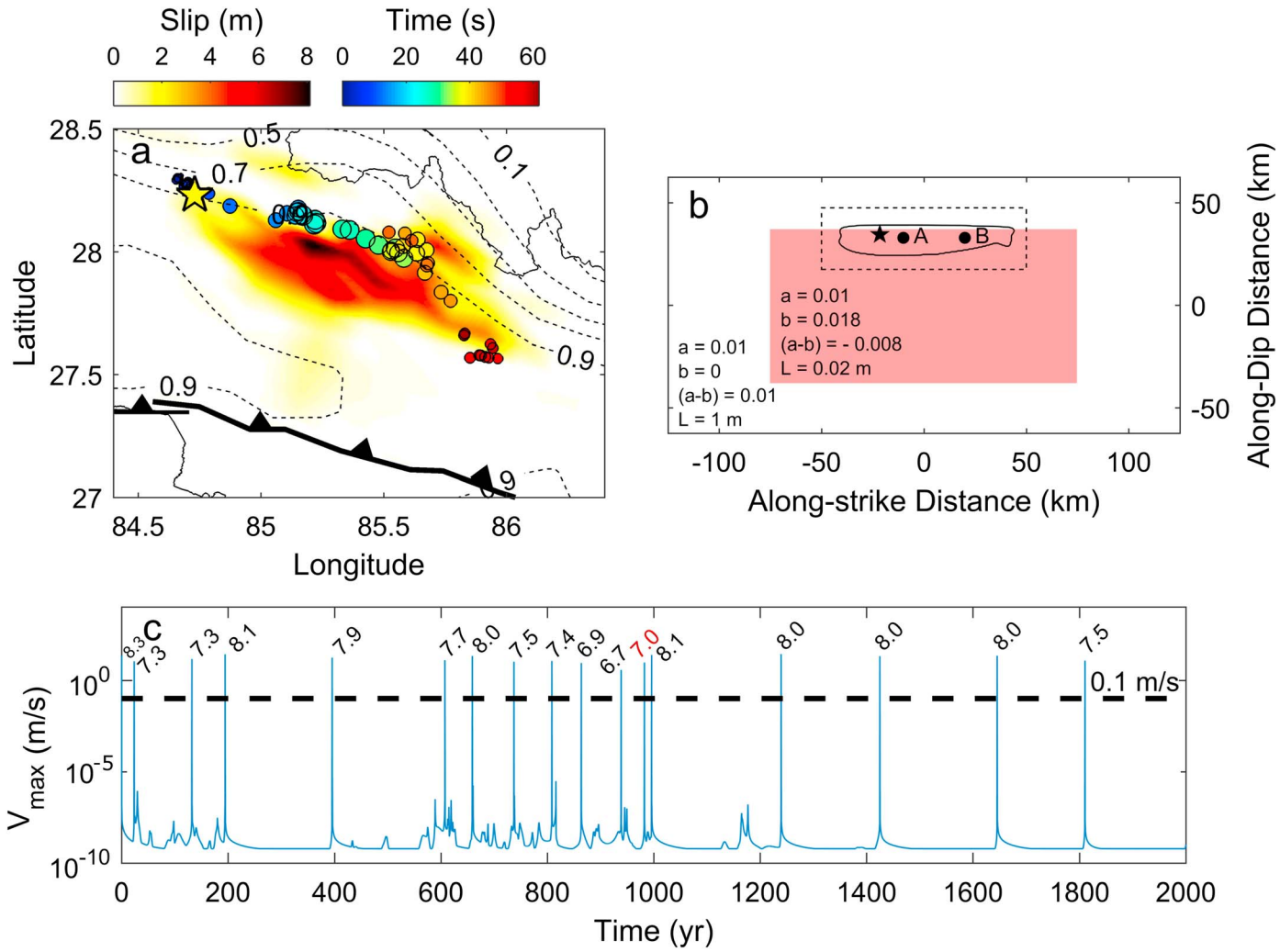

Figure 1. Setting of the *Mw*7.8 Gorkha earthquake and dynamic simulations presented in this study. (a) Distribution of coseismic slip, location, and timing of the sources of high-frequency radiations (0.5–2 Hz) and pattern of interseismic coupling on the Main Himalayan Thrust fault (isocontour of locking from 10% to 90%) [*Avouac et al.*, 2015; *Galetzka et al.*, 2015; *Stevens and Avouac*, 2015; *Elliott et al.*, 2016]. (b) Our fault model, with the velocity-strengthening (VS) and velocity-weakening (VW) areas indicated by the white and pink areas, respectively. The fault is loaded by dip-slip motion (slip is parallel to the shorter dimension of the model). The solid black line and black star represent the rupture area and epicenter of event 12, respectively. The black dashed rectangle outlines the area shown in Figure 2. The black dots show the location of points A and B where slip and stress histories are shown in Figure 3. (c) Maximum slip rate as a function of time during the 2000 yearlong simulation. The dashed horizontal line shows the 0.1 m/s threshold above which slip is considered to be seismic. Magnitudes are indicated, with event 12 in red.

[*Barbot et al.*, 2012; *Cubas et al.*, 2015; *Thomas et al.*, 2017]. We assume that the state variable evolves according to the "aging law" [*Dieterich*, 1972, 1979; *Ruina*, 1983]. The frictional resistance is then expressed as

$$\tau = \sigma\left[f_* + a\,\ln\left(\frac{V}{V_*}\right) + b\,\ln\left(\frac{V_*\,\theta}{L}\right)\right], \tag{1a}$$

$$\frac{d\theta}{dt} = 1 - \frac{V\,\theta}{L}, \tag{1b}$$

where τ is the shear strength which is equal to the shear stress, σ is the effective normal stress, V is the slip rate, and f_* is the friction coefficient at the reference slip rate V_*. The parameter a quantifies the direct effect of a slip-rate change. The parameter b describes the effect of the state variable. The characteristic slip distance, L, governs the evolution of the state variable. Friction is said to be velocity weakening (VW) if $a - b < 0$, and velocity-strengthening (VS) if $a - b > 0$. A VW behavior of the fault is required for seismic

Table 1. List of Physical Parameters Used in the Model

	Symbol	Value
	Elastodynamic Properties	
Shear modulus	μ	30 GPa
Poisson's ratio	ν	0.25
Shear wave speed	c_s	3 km/s
	Frictional Properties	
Reference slip rate	V_*	1 μm/s
Reference friction coefficient	f_*	0.6
Characteristic slip distance	L	20 mm in VW region 1 m in VS area
Direct effect parameter	a	0.01
Evolution effect parameter	b	0.018 in VW region 0 in VS area
	Other model parameters	
Effective normal stress	σ	50 MPa
Plate loading rate	V_{pl}	21 mm/yr

ruptures to nucleate. In dynamic simulations, VW patches produce a stick-slip motion, if they are larger than the critical size for earthquake nucleation, i.e., the nucleation size, h^* [*Ampuero and Rubin*, 2008; *Chen and Lapusta*, 2009]:

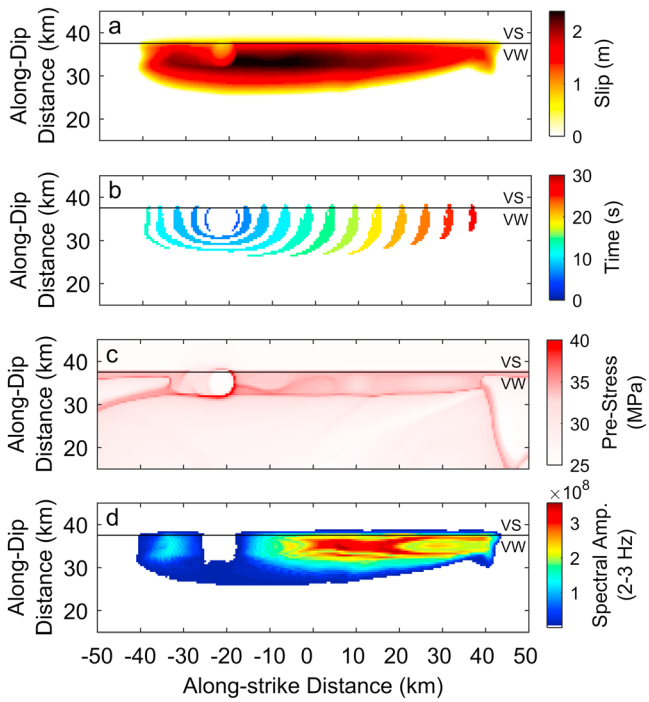

Figure 2. Cumulative slip, rupture front propagation, shear prestress, and high-frequency radiation spatial maps of a partial rupture (event 12). (a) Cumulative slip and (b) rupture front propagation of the event. In Figure 2b, the lines show, at 2 s time intervals, location where slip rate exceeds 0.5 m/s, with their color indicating the timing during the rupture. (c) Shear stress at the onset of seismic event, defined as the slip rate exceeding 0.1 m/s somewhere on the fault. The stress has already dropped where nucleation has been occurring. The color scale is saturated to better visualize the stress distribution. The maximum and minimum shear stress on the fault are 47 MPa and 24 MPa, respectively. (d) Map of high-frequency sources during the rupture. Color shading shows the amplitude of the spectrum of the slip-time function between 2 and 3 Hz. The solid black horizontal line is the boundary between the VS and VW areas.

$$h^* = \frac{\pi}{2}\frac{\mu^* bL}{(b-a)^2\sigma}, \qquad (2)$$

where $\mu^* = \mu$ for mode III, and $\mu^* = \mu/(1-\nu)$ for mode II, with μ and ν being the shear modulus and Poisson ratio, respectively. Accordingly, smaller L values allow for smaller h^* and hence simulations of smaller earthquakes, thereby producing a broader range of earthquake magnitudes and adding further complexity to earthquake sequences. However, this comes at a computational cost.

We design a simple generic experiment meant to reproduce a single fault. We therefore consider only one homogeneous VW patch embedded in a VS area (Figure 1b). The model is not aimed to reproduce any particular detail of the MHT. For simplicity, we assume a constant effective normal stress.

The physical parameters used in this study are listed in Table 1. The parameters were chosen to keep the computational cost of the simulations reasonable. The modeled fault is 250 km long along strike and 125 km wide along dip, and the VW region is 150 km long and 75 km wide. With the assumed parameters (Table 1), the nucleation size is ~5 km. The fault is loaded at a rate of 21 mm/yr

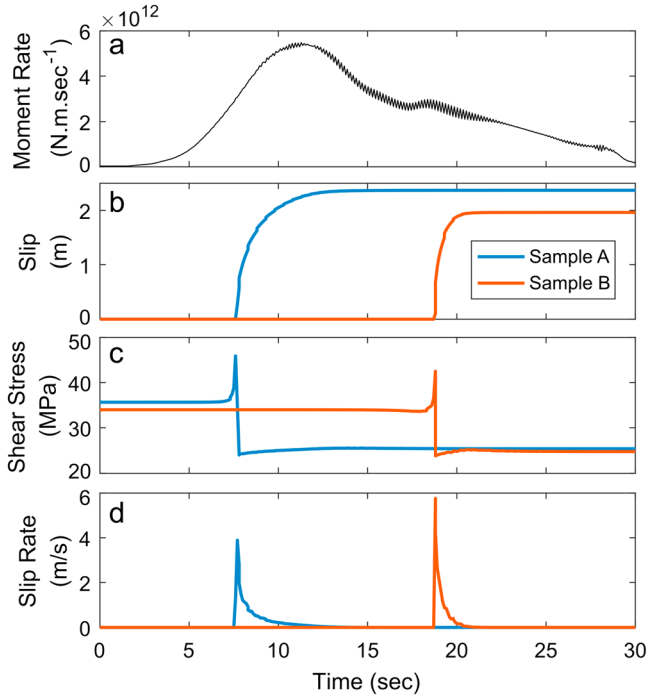

Figure 3. (a) Source-time function (moment rate as a function of time) of the partial rupture (event 12). (b) Cumulative slip, (c) shear prestress, and (d) slip rate at the locations of points A and B from Figure 1b.

perpendicular to the strike direction. Note that the loading is applied all around the frictional region (there is no free surface) so that all edges of the VW region will consequently concentrate stress during the interseismic period (not just the bottom edge). The effective normal stress is set at 50 MPa. The simulation starts with an earthquake artificially triggered by elevated shear stresses within a 20 km by 20 km area located at the edge of the VW region. The first several earthquakes reset the model from the initial imposed conditions on the fault.

3. Modeling Results

The simulation produces a sequence of full and partial ruptures of the VW region, with 17 events (defined as slip with $V > 0.1$ m/s) occurring in 2000 years, their magnitudes ranging from 6.7 to 8.3 (Figure 1c). We observe that earthquakes nucleate at the edges of the VW patch where stress builds up more rapidly. The largest events ($M_w > 7.9$) generally rupture nearly entirely the VW area. We observe that partial ruptures are systematically confined along the edge of the VW region (supporting information) where preseismic stresses are higher due to interseismic stress buildup.

We present details of such a partial rupture, event 12 (Figures 1b and 1c), in Figures 2 and 3 (a video is available in the supporting information). This earthquake reaches a moment magnitude M_w7 and produces an average stress drop of 6.15 MPa (calculated using the spatial average of stress drop distribution approach of *Noda et al*. [2013]). This partial rupture unzips the edge of the VW area over an along-strike length of about 80 km, producing a peak slip of 2.4 m (Figure 2a). The earthquake nucleates in a particularly wide zone of higher prestress. The rupture is initially crack-like for about 8–10 s and then turns into a unilateral pulse-like rupture until the end of the rupture, for another 20 s (Figure 2b). The source time function (e.g., the time evolution of the moment rate released by the entire rupture) peaks at ~11 s after the onset of seismic velocities (Figure 3a). The peak moment rate occurs approximately when the rupture area stops expanding along dip. This arrest is at the origin of the healing front that leads to a pulse-like behavior. From there on, the moment rate decreases gradually.

The comparison of the source-time function (Figure 3a) with the slip-time functions at points A and B (Figure 3b and c) shows that the slip pulse duration at these points, equal to ~5 s, is small compared to the ~30 s source duration. Most (>95%) of the final slip is reached much before the end of the rupture. The evolution of slip thus attests to a pulse-like behavior. Seven seconds after the start of the event, the rupture propagates along strike at a mean rupture speed of 2.700 ± 0.002 km/s (the uncertainty is the standard deviation), which is about 90% of the Rayleigh wave speed.

Comparison of the slip accumulation (Figure 2a) with the distribution of shear stress on the fault prior to the rupture (Figure 2c) suggests that the width of the rupture is determined by the extent of the higher shear prestress at the edge of the VW region and its decrease toward lower stress values in the middle of the fault. Along strike, the rupture arrests at zones of lower stress that have been ruptured by recent prior earthquakes.

We observe that the evolution of slip rate is sharper at points near the edge of the VW area, probably due to the higher shear stress there (Figure 2c). This effect results in relatively more energetic high-frequency seismic waves radiated from near the edge of the VW area (supporting information). To quantify this

effect, we compute the Fourier transform of the moment-rate time function and assess spatial variations of the amplitude of the spectrum at frequencies between 2 and 3 Hz (Figure 3d).

Note that the sequence of partial and full ruptures is only possible if the nucleation size is small enough compared to the width of the VW region (supporting information). By changing the width of the seismogenic zone, we find that only full ruptures occur if the ratio between the nucleation size and the width of the VW region is above 1/12. This particular value may be linked to the frictional parameters and geometry chosen in this study and its dependence on these factors requires further study, although we expect that, in any fault model, this value needs to be small enough for the partial ruptures to appear.

4. Discussion and Conclusion

A simple model based on standard rate-and-state friction with a single homogeneous VW patch surrounded by a VS region and loaded with dip-slip motion can produce partial ruptures that unzip the edge of the VW zone. This kind of rupture was observed in the continental context of the Himalayan megathrust during the *M*7.8 Gorkha earthquake, and in the context of oceanic subduction zones [*Pritchard et al*., 2007; *Béjar-Pizarro et al*., 2010]. Such ruptures could also result from a structural control by the fault geometry or from spatial variations of friction properties. In the case of the Gorkha earthquake, the hypothesis that the upper edge of the rupture was controlled by a transition to VS friction can be excluded based on postseismic observations, which show that the area updip of the seismic rupture remains locked [*Gualandi et al*., 2016]. By contrast, there is a possibility that the upper edge of the Gorkha earthquake was controlled by a ramp [*Hubbard et al*., 2016; *Qiu et al*., 2016]. This ramp would run beneath the Kathmandu basin. There is, however, no topographic signature of the zone of more rapid uplift that should have resulted.

We therefore prefer the alternative scenario, suggested by the partial ruptures observed in our numerical simulations, that the rupture was confined to the area of interseismic stress buildup at the lower edge of the locked area. This hypothesis could also explain similar ruptures in the context of oceanic subductions.

The pulse-like behavior in our simulated partial ruptures is controlled by the width of the zone within which seismic slip can be sustained due to the stress distribution. Pulse-like ruptures, often observed in various tectonic settings [*Heaton*, 1990], can hence form as a result of the stress concentration at the boundary between VW and VS zone, or at any other band of concentrated stress. Hence, they do not necessarily require a narrow or heterogeneous seismogenic zones [*Johnson*, 1992; *Beroza and Mikumo*, 1996; *Olsen et al*., 1997], intense frictional velocity weakening [*Heaton*, 1990; *Lu et al*., 2007], or elastic contrast across the fault [*Ampuero and Ben-Zion*, 2008] although such features may be present and indeed required for slip in certain settings, e.g., on low-stressed faults of high static strength [*Zheng and Rice*, 1998; *Noda et al*., 2009].

In our model, the sources of dominant high-frequency radiation are at the locations of high pre-seismic shear stress, whether it is a partial or full rupture (an example of full rupture is given in the supporting information). The high-frequency radiation sources of the Gorkha earthquake are located downdip, close to the transition between the VS and VW region, as in our model. While our model succeeds at explaining the location of the high-frequency sources, the effect might actually be stronger in nature than what our model predicts. Indeed, for computational reasons, the nucleation size of our modeled earthquakes is relatively large, leading only to $M_w > 6$ events. In nature, seismic ruptures can be much smaller. In our model, earthquakes tend to nucleate at the edges of the VW patch where stress is building up more rapidly. This result is similar to the observations that most earthquakes in the Himalaya cluster along the lower edge of the locked fault zone [*Cattin and Avouac*, 2000; *Bollinger et al*., 2004; *Stevens and Avouac*, 2015]. It is likely that due to these smaller earthquakes, the stress distribution along the lower edge of the VW zone is much more heterogeneous than in our model [*Lapusta and Rice*, 2003; *Jiang and Lapusta*, 2016]. If the simulated earthquakes could span smaller magnitudes, it would enhance further the high-frequency seismic waves radiated from the edge of the VW area [*Avouac et al*., 2015]. Our explanation for the locations of the HF sources does not exclude the alternative possibility that they coincide with the upper edge of the midcrustal ramp along the Himalayan megathrust [*Elliott et al*., 2016], which coincides with the steep topography and the zone of higher exhumation rate at the front of the Higher Himalaya [*Lavé and Avouac*, 2001; *Herman et al*., 2010]. It is indeed well known that high-frequency waves are radiated at fault kinks [e.g., *Adda-Bedia and Madariaga*, 2008]. In the case of the Gorkha earthquake, no high-frequency radiation was

observed at its updip extent, a feature that should have been detected if the rupture had reached an updip additional ramp.

Our model does not imply that dominant high-frequency waves would only radiate from the edges of VW areas. The rupture of a zone of higher stress left at the edges of a previous partial rupture may dominate the HF radiation, which could then originate from well within the VW area. It is therefore not assured that seismic slip within the locked portion of megathrust would be depleted in high frequencies as a result of the mechanism described in this study. Further investigations are needed to elucidate the factors controlling the source location and amplitudes of high-frequency seismic waves.

Acknowledgments
The data used are listed in the supporting information. We thank Yen-Yu Lin for his help with the numerical code. We thank Adriano Gualandi, James Jackson, and Alex Copley for discussions. This research was partially funded by the National Science Fundation throuh grant EAR 1345136.

References

Adda-Bedia, M., and R. Madariaga (2008), Seismic radiation from a kink on an antiplane fault, *Bull. Seismol. Soc. Am.*, *98*(5), 2291–2302, doi:10.1785/0120080003.

Ampuero, J., and A. M. Rubin (2008), Earthquake nucleation on rate and state faults—Aging and slip laws, *J. Geophys. Res.*, *113*, B01302, doi:10.1029/2007JB005082.

Ampuero, J.-P., and Y. Ben-Zion (2008), Cracks, pulses and macroscopic asymmetry of dynamic rupture on a bimaterial interface with velocity-weakening friction, *Geophys. J. Int.*, *173*, 674–692, doi:10.1111/j.1365-246X.2008.03736.x.

Avouac, J., L. Meng, S. Wei, T. Wang, and J. Ampuero (2015), Lower edge of locked Main Himalayan Thrust unzipped by the 2015 Gorkha earthquake, *Nat. Geosci.*, *8*, 708–711, doi:10.1038/NGEO2518.

Barbot, S., N. Lapusta, and J. Avouac (2012), Under the hood of the earthquake, *Science*, *336*(6082), 707–710, doi:10.1126/science.1218796.

Béjar-Pizarro, M., et al. (2010), Asperities and barriers on the seismogenic zone in North Chile: State-of-the-art after the 2007 *Mw* 7.7 Tocopilla earthquake inferred by GPS and InSAR data, *Geophys. J. Int.*, *183*, 390–406, doi:10.1111/j.1365-246X.2010.04748.x.

Beroza, G. C., and T. Mikumo (1996), Short slip duration in dynamic rupture in the presence of heterogeneous fault properties, *J. Geogr. Geol.*, *101*, 22,449–22,460.

Bollinger, L., J. P. Avouac, R. Cattin, and M. R. Pandey (2004), Stress buildup in the Himalaya, *J. Geophys. Res.*, *109*, B11405, doi:10.1029/2003JB002911.

Cattin, R., and J. P. Avouac (2000), Modeling mountain building and the seismic cycle in the Himalaya of Nepal, *J. Geophys. Res.*, *105*, 13,989–13,407, doi:10.1029/2000JB900032.

Chen, T., and N. Lapusta (2009), Scaling of small repeating earthquakes explained by interaction of seismic and aseismic slip in a rate and state fault model, *J. Geophys. Res.*, *114*, B01311, doi:10.1029/2008JB005749.

Cubas, N., N. Lapusta, J. Avouac, and H. Perfettini (2015), Numerical modeling of long-term earthquake sequences on the NE Japan megathrust: Comparison with observations and implications for fault friction, *Earth Planet. Sci. Lett.*, *419*, 187–198, doi:10.1016/j.epsl.2015.03.002.

Dieterich, J. H. (1972), Time-dependent friction in rocks, *J. Geophys. Res.*, *77*, 3690–3697, doi:10.1029/JB077i020p03690.

Dieterich, J. H. (1979), Modeling of rock friction experimental results and constitutive equations, *J. Geophys. Res.*, *84*, 2161–2168, doi:10.1029/JB084iB05p02161.

Elliott, J. R., R. Jolivet, P. J. González, J. Avouac, J. Hollingsworth, and M. P. Searle (2016), Himalayan megathrust geometry and relation to topography revealed by the Gorkha earthquake, *Nat. Geosci.*, *9*, 174–180, doi:10.1038/NGEO2623.

Galetzka, J., et al. (2015), Slip pulse and resonance of the Kathmandu basin during the 2015 Gorkha earthquake, Nepal, *Science*, *349*(6252), 1091–1095.

Gualandi, A., J. Avouac, J. Galetzka, J. F. Genrich, G. Blewitt, and L. B. Adhikari (2016), Pre- and post-seismic deformation related to the 2015, *Mw*7.8 Gorkha earthquake, Nepal, *Tectonophysics*, doi:10.1016/j.tecto.2016.06.014.

Heaton, T. H. (1990), Evidence for and implications of self-healing pulses of slip in earthquake rupture, *Phys. Earth Planet. Inter.*, *64*, 1–20.

Herman, F., et al. (2010), Exhumation, crustal deformation, and thermal structure of the Nepal Himalaya derived from the inversion of thermochronological and thermobarometric data and modeling of the topography, *J. Geophys. Res.*, *115*, B06407, doi:10.1029/2008JB006126.

Hubbard, J., R. Almeida, A. Foster, S. N. Sapkota, P. Bürgi, and P. Tapponnier (2016), Structural segmentation controlled the 2015 *Mw* 7. 8 Gorkha earthquake rupture in Nepal, *Geology*, *44*(8), 639–642, doi:10.1130/G38077.1.

Jiang, J., and N. Lapusta (2016), Deeper penetration of large earthquakes on seismically quiescent faults, *Science*, *352*(6291), 1293–1298.

Johnson, E. (1992), The influence of the lithospheric thickness, *Geophys. J. Int.*, *108*, 151–160.

Konca, A. O., et al. (2008), Partial rupture of a locked patch of the Sumatra megathrust during the 2007 earthquake sequence, *Nature*, *456*, 631–635, doi:10.1038/nature07572.

Lapusta, N., and Y. Liu (2009), Three-dimensional boundary integral modeling of spontaneous earthquake sequences and aseismic slip, *J. Geophys. Res.*, *114*, B09303, doi:10.1029/2008JB005934.

Lapusta, N., and J. R. Rice (2003), Nucleation and early seismic propagation of small and large events in a crustal earthquake model, *J. Geophys. Res.*, *108*(B4), 2205, doi:10.1029/2001JB000793.

Lavé, J., and J. P. Avouac (2001), Fluvial incision and tectonic uplift across the Himalayas of central Nepal, *J. Geophys. Res.*, *106*, 26,561–26,591, doi:10.1029/2001JB000359.

Loveless, J. P., and B. J. Meade (2011), Spatial correlation of interseismic coupling and coseismic rupture extent of the 2011 *Mw* = 9.0 Tohoku-oki earthquake, *Geophys. Res. Lett.*, *38*, L17306, doi:10.1029/2011GL048561.

Lu, X., N. Lapusta, and A. J. Rosakis (2007), Pulse-like and crack-like ruptures in experiments mimicking crustal earthquakes, *Proc. Natl. Acad. Sci. U.S.A.*, *104*(48), 18,931–18,936.

Meng, L., A. Zhang, and Y. Yagi (2016), Improving back projection imaging with a novel physics-based aftershock calibration approach: A case study of the 2015 Gorkha earthquake, *Geophys. Res. Lett.*, *43*, 628–636, doi:10.1002/2015GL067034.

Moreno, M., M. Rosenau, and O. Oncken (2010), 2010 Maule earthquake slip correlates with pre-seismic locking of Andean subduction zone, *Nature*, *467*, 198–202, doi:10.1038/nature09349.

Noda, H., E. M. Dunham, and J. R. Rice (2009), Earthquake ruptures with thermal weakening and the operation of major faults at low overall stress levels, *J. Geophys. Res.*, *114*, B07302, doi:10.1029/2008JB006143.

Noda, H., N. Lapusta, and H. Kanamori (2013), Comparison of average stress drop measures for ruptures with heterogeneous stress change and implications for earthquake physics, *Geophys. J. Int.*, *193*, 1691–1712, doi:10.1093/gji/ggt074.

Olsen, K. B., R. Madariaga, and R. J. Archuleta (1997), Three-dimensional dynamic simulation of the 1992 Landers earthquake, *Science*, *278*(5339), 834–838, doi:10.1126/science.278.5339.834.

Pritchard, M. E., E. O. Norabuena, C. Ji, R. Boroschek, D. Comte, M. Simons, T. H. Dixon, and P. A. Rosen (2007), Geodetic, teleseismic, and strong motion constraints on slip from recent southern Peru subduction zone earthquakes, *J. Geophys. Res.*, *112*, B03307, doi:10.1029/2006JB004294.

Protti, M., V. González, A. V. Newman, T. H. Dixon, S. Y. Schwartz, J. S. Marshall, L. Feng, J. I. Walter, R. Malservisi, and S. E. Owen (2013), Nicoya earthquake rupture anticipated by geodetic measurement of the locked plate interface, *Nat. Geosci.*, *7*, 117–121, doi:10.1038/ngeo2038.

Qiu, Q., E. M. Hill, S. Barbot, J. Hubbard, W. Feng, E. O. Lindsey, L. Feng, K. Dai, S. V. Samsonov, and P. Tapponnier (2016), The mechanism of partial rupture of a locked megathrust: The role of fault morphology, *Geol. Soc. Am.*, *44*(10), 875–878, doi:10.1130/G38178.1.

Ruina, A. (1983), Slip instability and state variable friction laws, *J. Geophys. Res.*, *88*, 10,359–10,370, doi:10.1029/JB088iB12p10359.

Stevens, V. L., and J. P. Avouac (2015), Interseismic coupling on the Main Himalayan Thrust, *Geophys. Res. Lett.*, *42*, 5828–5837, doi:10.1002/2015GL064845.

Thomas, M. Y., J. Avouac, and N. Lapusta (2017), Rate-and-state friction properties of the Longitudinal Valley fault from kinematic and dynamic modeling of seismic and aseismic slip, *J. Geophys. Res. Solid Earth*, *122*, 3115–3137, doi:10.1002/2016JB013615.

Zheng, G., and J. R. Rice (1998), Conditions under which velocity-weakening friction allows a self-healing versus a cracklike mode of rupture, *Bull. Seismol. Soc. Am.*, *88*(6), 1466–1483.